Lipase B Immobilized Silica-coated Magnetic Nanoparticles for Rapid Hydrolysis, Acylation, and Lipolysis

Yu Jeong Kim and JEONG HO CHANG *

Posted Date: 9 August 2024

doi: 10.20944/preprints202408.0671.v1

Keywords: Lipase, Immobilization; Magnetic nanoparticles; Lipolysis; Acylation; Hydrolysis

 doi:10.20944/preprints202408.0671.v1

Article

Lipase B Immobilized Silica-Coated Magnetic Nanoparticles for Rapid Hydrolysis, Acylation, and Lipolysis

Yu Jeong Kim and Jeong Ho Chang *

Korea Institute of Ceramic Engineering and Technology, Chungbuk 28160, Republic of Korea

* Correspondence: author: jhchang@kicet.re.kr (J.H. Chang). ***Phone:*** +82 43 913 1510

Abstract: This study reports rapid hydrolysis, acylation, and lipolysis with lipase B from *Candida antarctica* (CalB) and nanofructosome encapsulated CalB (CalB@NF) enzymes immobilized on silica-coated magnetic nanoparticles (Si-MNPs). Enzymatic hydrolysis was confirmed for conversion to *p*-nitrophenol (*p*-NP, λ_{ex}=400 nm) from *p*-nitrophenyl butyrate (*p*-NPB, λ_{ex}=270 nm), and various catalytic parameters such as K_m, V_{max}, and K_{cat} were calculated from Michaelis-Menten and Lineweaver-Burk plot. Efficiency of enzymatic hydrolysis was in the order of CalB > Si-MNPs@CalB > CalB@NF > Si-MNPs@CalB@NF, and reusability was much better with the enzyme immobilized on Si-MNPs than with the native enzyme. Enzymatic acylation was confirmed by the formation of benzyl benzoate (λ_{ex}=229 nm) from benzoic anhydride (λ_{ex}=240 nm), and efficiency exceeded 99% in all samples. Finally, enzymatic lipolysis was confirmed by the decomposition of olive oil to fatty acid such as oleic acid (λ_{ex}=230 nm) using thin-layer chromatography (TLC), column chromatography, and proton nuclear magnetic resonance (^{1}H -NMR). The lipases immobilized on Si-MNPs have the advantage of good thermal stability and reusability and are thus applicable to a wide range of industries.

Keywords: lipase; immobilization; magnetic nanoparticles; lipolysis; acylation; hydrolysis

1. Introduction

Lipases are most commonly used for a wide range of reactions including interesterification, transesterification, alcoholysis, acidolysis and aminolysis [1–7]. They are employed in various industrial applications, including in the chemical industry [8], cosmetics [9], biodegradation [10], detergents [11], leather processing [12], fuel production [13], biodiesel [14], flavor esters [15], and structured lipids [16]. Lipase catalysts are highly valued industrially because they have high activity and substrate specificity compared to chemical catalysts and operate under mild conditions (temperature and pH) [17].

Among lipases, the enzyme lipase B from *Candida antarctica* (CalB) is widely used in industry and other practical applications due to properties such as extensive substrate specificity, good stereoselectivity, chemical compatibility and stability [18]. However, CalB is expensive for industrial use, and its low resistance to organic solvents and sensitivity to temperature changes make it difficult to store [19]. To address this, various methods have been developed to immobilize CalB [20]. The most commercially used CalB is Novozyme® 435, which is immobilized in acrylic resin [21]. However, the enzyme is very expensive due to the high unit cost of the acrylic resin used for immobilization, the release of the enzyme from certain media due to the acrylic resin, and the dissolution of the acrylic resin in organic media. In addition, enzymes immobilized on acrylic supports require additional separation steps such as centrifugation and filtration, which add to the process time [22,23].

To solve this problem, the CalB enzyme was immobilized with levan. Levan is a water-soluble fructan composed of fructose molecules linked by β-2,6 glycosides and is a natural polysaccharide found in certain microbial and plant species [24]. In addition, it has a low intrinsic viscosity compared

 doi:10.20944/preprints202408.0671.v1

to other polysaccharides of similar molecular weight and exhibits thermal stability in acidic and alkaline media [25]. Therefore, when CalB is immobilized on levan, it is very stable under temperature changes and retains high activity even in long-term processes [26,27].

Recently, it has been reported that lipases can be immobilized using a variety of solid supports, including silica [28,29], polymers [30], carbon [31], metals [32], and magnetic particles [33,34]. Among magnetic nanoparticles, Fe_3O_4 can be used for enzyme immobilization due to its suitable magnetic properties, which facilitate recovery with magnets and greatly reduce separation time [35–37]. However, magnetic nanoparticles are susceptible to rusting and corrosion in aqueous solutions, which constrains their functionalization for binding biomolecules. Silica coating on magnetic nanoparticles prevents rusting, maintains magnetism, and facilitates bonding due to the abundance of hydroxyl groups (-OH) [38]. In addition, silica-coated magnetic nanoparticles can be easily functionalized with different functional groups to form chemical bonds with enzymes during the immobilization process [39,40].

In the present study, Si-MNPs were used as immobilization supports to CalB and CalB@NF enzymes for rapid recovery and reuse, as well as hydrolysis, acylation, and lipolysis. In addition, it was demonstrated that surface modification with chlorosilane on silica-coated magnetic nanoparticles enhance the immobilization efficiency of CalB and CalB@NF enzymes (Scheme 1a). The materials were also evaluated for thermal stability and pH stability at 25-65°C and pH 5-9, and Bradford assay and TGA analysis were performed to analyze the content of CalB in each sample. The hydrolysis and acylation reactions were confirmed by the formation of *p*-nitrophenyl butyrate (*p*-NPB) and benzyl benzoate. Moreover, hydrolytic parameters such as K_m, V_{max} and K_{cat} were calculated using the Michaelis-Menten equation and Lineweaver-Burk plots, and acylation efficiency was calculated via benzyl benzoate synthesis from benzoic anhydride. Lipolysis was confirmed the formation of fatty acids such as oleic acid from olive oil (Scheme 1b).

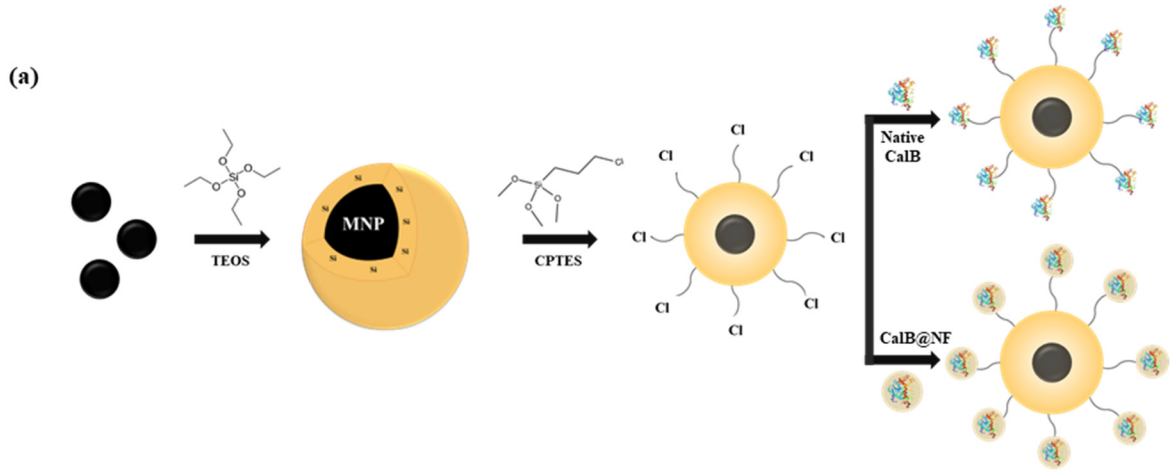

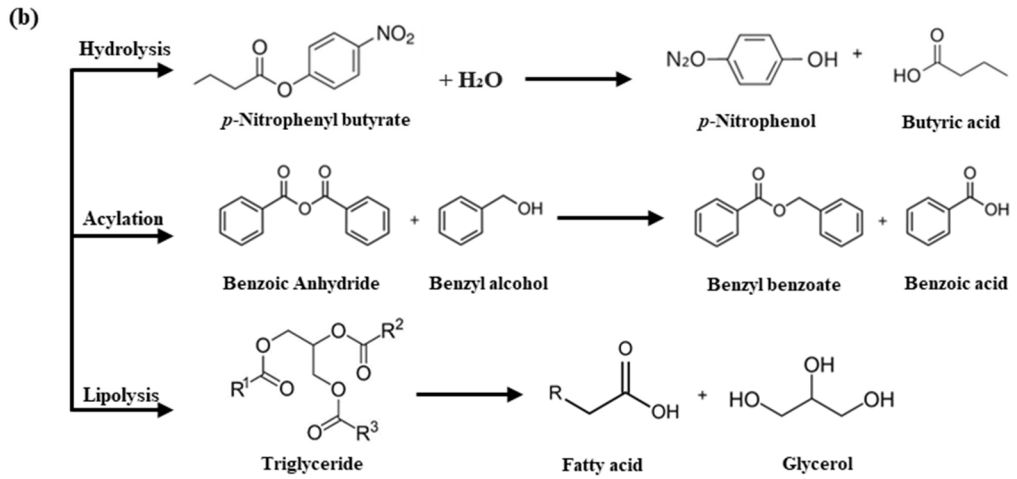

 doi:10.20944/preprints202408.0671.v1

Scheme 1. (a) Scheme for CalB and CalB@NF immobilization on Si-MNPs through chloro-silane modification, and (b) enzymatic reaction for hydrolysis, acylation, and lipolysis with the prepared samples.

2. Results and Discussion

2.1. Preparation and Characterization of Si-MNPs and Si-MNPs@Cl

Figure 1 shows the characterization of magnetic nanoparticles (MNPs), silica-coated magnetic nanoparticles (Si-MNPs), chlorosilane cross-linked Si-MNPs, and native CalB and CalB@NF lipase immobilized on Si-MNPs@Cl (Si-MNPs@CalB, and Si-MNPs@CalB@NF), respectively. MNPs were synthesized by the coprecipitation method, and the particle surface was coated with silica by a sol-gel method using tetraethyl orthosilicate (TEOS) as a silica precursor [41]. Figure 1a shows transmission electron microscopy (TEM) to confirm the morphological details and particle size of MNPs and Si-MNPs. The TEM was measured at 80,000x magnification and confirmed that the MNPs have an average size of 17 nm and a polygonal shape. Si-MNPs were also identified in the same multiples and confirmed to have an average size of 60 nm with a 43 nm shell coated in a spherical shape. Figure 1b shows vibrating sample magnetometer (VSM) measurements of MNPs and Si-MNPs. The magnetic susceptibility of MNPs and Si-MNPs is 0.59442 $emug^{-1}$ and 0.3387 $emug^{-1}$ at 300 K, respectively. Moreover, the magnetic susceptibility of Si-MNPs were observed to be easily magnetically separated within 1 minute when dispersed in water by shaking or sonication. The lower magnetic susceptibility of Si-MNPs compared to MNPs is attributed to the silica coating. X-ray diffraction (XRD) and Fourier transform-infrared (FT-IR) were then used to identify the shells coated on the MNPs in Figure 1b,c. Figure 1b shows the XRD data of MNPs and Si-MNPs. The MNPs showed diffraction peaks at 2θ = 35.4°, 57.3°, and 63.2°, which can be attributed to the Fe_3O_4 planes (311), (511), and (400) of the MNPs, respectively. The XRD peak of Si-MNPs is consistent with the pattern of Fe_3O_4, while Si-MNPs show broad peaks at low diffraction angles between 20°-27°, indicating an amorphous SiO_2 shell coating the MNPs. The XRD pattern of Si-MNPs exhibited significantly lower intensity peaks attributable to the MNPs core. This was due to the coating of the amorphous silica shell. Figure 1c shows the FT-IR results of MNPs, Si-MNPs, and Si-MNPs@Cl. For the MNPs, Fe-O and O-H bonds at 750 cm^{-1} and 3400 cm^{-1} peaks were confirmed. Similarly, the silica coating was confirmed for the Si-MNPs by identifying Fe-O and O-H bonds at 750 cm^{-1} and 3400 cm^{-1} peaks and Si-O bonds at a 1090 cm^{-1} peak that were not present in MNPs. XRD and FT-IR analyses confirmed that the coating identified as silica on the MNPs by TEM was indeed silica. Furthermore, these analyses confirmed that the intrinsic properties of the MNPs remained intact despite the silica coating on the MNPs. Coating MNPs with silica serves to prevents rusting and loss of magnetism in aqueous solutions. In addition, the abundance of -OH groups on the silica surface facilitates enzyme immobilization. Therefore, Si-MNPs were used instead of direct immobilization of the enzyme on MNPs. In addition, the enzyme was not immobilized directly on the Si-MNPs, but surface treated with chlorosilane. FT-IR of Si-MNPs@Cl with chloro-functionalized silane on Si-MNPs are shown. The silane used is 3-chloropropyltriethoxysilane (CPTES), which has many C-H vibrations. The C-H vibration of CPTES appears at 2915 cm^{-1} and was verified by FT-IR of Si-MNPs@Cl to confirm the surface treatment. Figure 1d shows the TGA analysis results of Si-MNPs@Cl, Si-MNPs@CalB, and Si-MNPs@CalB@NF. The amount of native CalB and CalB@NF for each conformational change were investigated by TGA in the temperature range of 200-700 °C. The amounts of native CalB and CalB@NF immobilized on Si-MNPs@Cl were 33.53% and 19.42%, respectively. Figure 1e shows the CalB quantification results of four samples (native CalB, CalB@NF, Si-MNPs@CalB, and Si-MNPs@CalB@NF) by a Bradford assay. The Bradford assay quantified the protein by measuring the absorbance at λ_{ex}=595 nm using UV-Vis. Quantification of the CalB content of 1 mg of each of the four samples showed that natural CalB contained 137.7 mg/mL while CalB@NF contained 20.6 mg/mL, representing a difference in content of more than seven-fold. In addition, Si-MNPs@CalB and Si-MNPs@CalB@NF contained 32 mg/mL and 16 mg/mL, respectively, representing a difference in content of more than two-fold.

 doi:10.20944/preprints202408.0671.v1

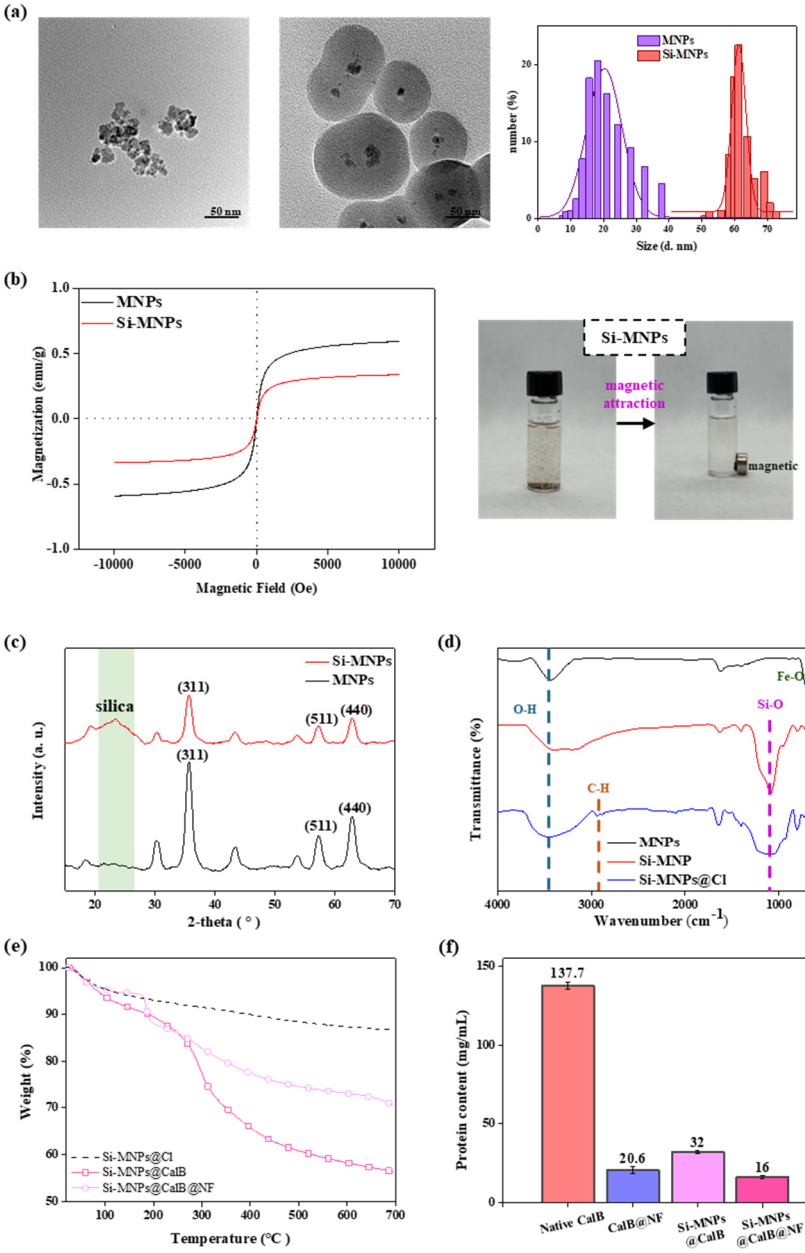

Figure 1. (a) TEM images of magnetic nanoparticles and silica-coated magnetic nanoparticles, (b) magnetic susceptibility of MNPs and Si-MNPs and images of magnetic attraction, (c)XRD spectra of MNPs and Si-MNPs, (d) FT-IR spectra of MNPs, Si-MNPs, and Si-MNPs@Cl, (e) TGA analysis of Si-MNPs@Cl,, Si-MNPs@CalB, and Si-MNPs@CalB@NF, (f) Bradford assay of native CalB, CalB@NF, Si-MNPs@CalB, and Si-MNPs@CalB@NF.

2.2. Enzymatic Hydrolysis

Figure 2a schematically presents the reaction for enzymatic hydrolysis of *p*-NPB to *p*-NP using four different samples (native CalB, CalB@NF, Si-MNPs@CalB, and Si-MNPs@CalB@NF). Figure 2b shows the reaction from *p*-NPB to *p*-NP as a function of time (1 min - 35 min) of Si-MNPs@CalB and Si-MNPs@CalB@NF to confirm enzymatic hydrolysis. The absorbance of the reactant *p*-NPB was measured at λ_{ex}=270 nm, while the absorbance of the product *p*-NP was measured at λ_{ex}=400 nm by UV-Vis spectrophotometer. As the reaction time increases, the absorbance of *p*-NPB (λ_{ex}=270 nm) decreases, and the absorbance of *p*-NP (λ_{ex}=400 nm) increases due to the catalytic action of Si-MNPs@CalB and Si-MNPs@CalB@NF. In addition, enzymatic hydrolysis confirmed that Si-MNPs@CalB occurs faster than Si-MNPs@CalB@NF. This indicates that during the hydrolysis of *p*-

 doi:10.20944/preprints202408.0671.v1

NPB to the product *p*-NP, the catalyst Si-MNPs@CalB reacts faster and more extensively than Si-MNPs@CalB@NF. This is because with a higher the amount of native CalB contained in the catalyst, an accordingly faster the catalytic reaction will occur. Figure 2c shows the Lineweaver-Burk plots of the four samples to determine the correlation between substrate and enzyme and to assess the catalytic efficiency. The Michaelis-Menten constant (K_m) indicates the affinity between the enzyme and the substrate, with lower values indicating that the enzyme binds more effectively to the substrate. The turnover rate (K_{cat}) refers to the number of times each enzyme site converts a substrate to a product per unit time. The K_{cat}/K_m ratio was used as a measure of enzyme performance. The enzyme kinetic parameters (K_m, V_{max}, and K_{cat}) calculated for the four samples are shown in Table 1. Native CalB has the highest Km value of 187 μM, indicating the lowest affinity for the substrate. The K_m values of CalB@NF, Si-MNPs@CalB, and Si-MNPs@CalB@NF were shown to be 94 μM, 139 μM, and 96 μM, respectively. Among the four samples, CalB@NF has the lowest K_m value because it has a good affinity for substrates due to the abundance of hydroxyl groups in levan and reacts well with substrates in aqueous solution. The K_m value of Si-MNPs@CalB@NF was also confirmed to be lower than that of native CalB and Si-MNPs@CalB. However, the V_{max} value of native CalB was 46 $\mu Mmin^{-1}$, and the values of CalB@NF, Si-MNPs@CalB, and Si-MNPs@CalB@NF decreased to 9 $\mu Mmin^{-1}$, 9.5 $\mu Mmin^{-1}$, and 4 $\mu Mmin^{-1}$, respectively, as the concentration of contained CalB decreased. V_{max} is proportional to the concentration of the enzyme. K_{cat} and K_{cat}/K_m results were calculated with K_m and V_{max} results. The K_{cat} values associated with the ability of the enzyme were 1393 min^{-1}, 1909 min^{-1}, 1151 min^{-1}, and 975 min^{-1} for native CalB, CalB@NF, Si-MNPs@CalB, and Si-MNPs@CalB@NF, respectively, falling in the order of CalB@NF > native CalB > Si-MNPs@CalB > Si-MNPs@CalB@NF. K_{cat}/K_m values, indicating the efficiency of the enzyme, were 7.4 $\mu M^{-1}min^{-1}$, 20.3 $\mu M^{-1}min^{-1}$, 8.3 $\mu M^{-1}min^{-1}$, and 10.2 $\mu M^{-1}min^{-1}$ for native CalB, CalB@NF, Si-MNPs@CalB, and Si-MNPs@CalB@NF, respectively, falling in the order of CalB@NF > Si-MNPs@CalB@NF > Si-MNPs@CalB > native CalB. The K_{cat} and K_{cat}/K_m ratios were highest for CalB@NF. This is because CalB@NF has a high affinity for substrates due to the presence of levan, allowing it to react effectively with substrates in aqueous solution. Figure 2d shows the catalytic activity at different pH conditions (5, 6, 7, 8, 9) for Si-MNPs@CalB and Si-MNPs@CalB@NF. The activity of Si-MNPs@CalB and Si-MNPs@CalB@NF was highest at pH 8, and the catalytic activity was confirmed to be up to 10% better for Si-MNPs@CalB@NF. Figure 2e shows the catalytic activity at different temperatures (25°C, 35°C, 45°C, 55°C and 65°C). The catalytic activity was found to be optimal at 45°C, with Si-MNPs@CalB@NF exhibiting approximately 20% better activity against temperature changes compared to Si-MNPs@CalB. This confirmed that using CalB@NF instead of native CalB provided greater stability changes in pH and temperature. It also means that the activity of the enzyme in response to changes in pH and temperature depends on its catalytic efficiency at specific pH and temperature conditions, regardless of encapsulation by levan. Thermal stability and pH activity are crucial factors in comprehending how lipase encapsulation influences enzyme activity. In other studies, as in this study, CalB@NF has been reported to exhibit higher thermal stability than native CalB [32]. Figure 2f shows the reusability results for the four samples. Reusability was evaluated by repeating the separation and washing process with a magnet for Si-MNPs@CalB and Si-MNPs@CalB@NF, while native CalB and CalB@NF were not recoverable. As the number of reuses increased, the catalytic activity decreased due to the difficulty of complete collection. Nevertheless, it was found that both Si-MNPs@CalB and Si-MNPs@CalB@NF showed more than 50% activity even after six reuses. Therefore, the enzymes immobilized on Si-MNPs@Cl (Si-MNPs@CalB and Si-MNPs@CalB@NF) can be reused repeatedly, enhancing process efficiency and reducing costs through their sustained use in industrial processes.

 doi:10.20944/preprints202408.0671.v1

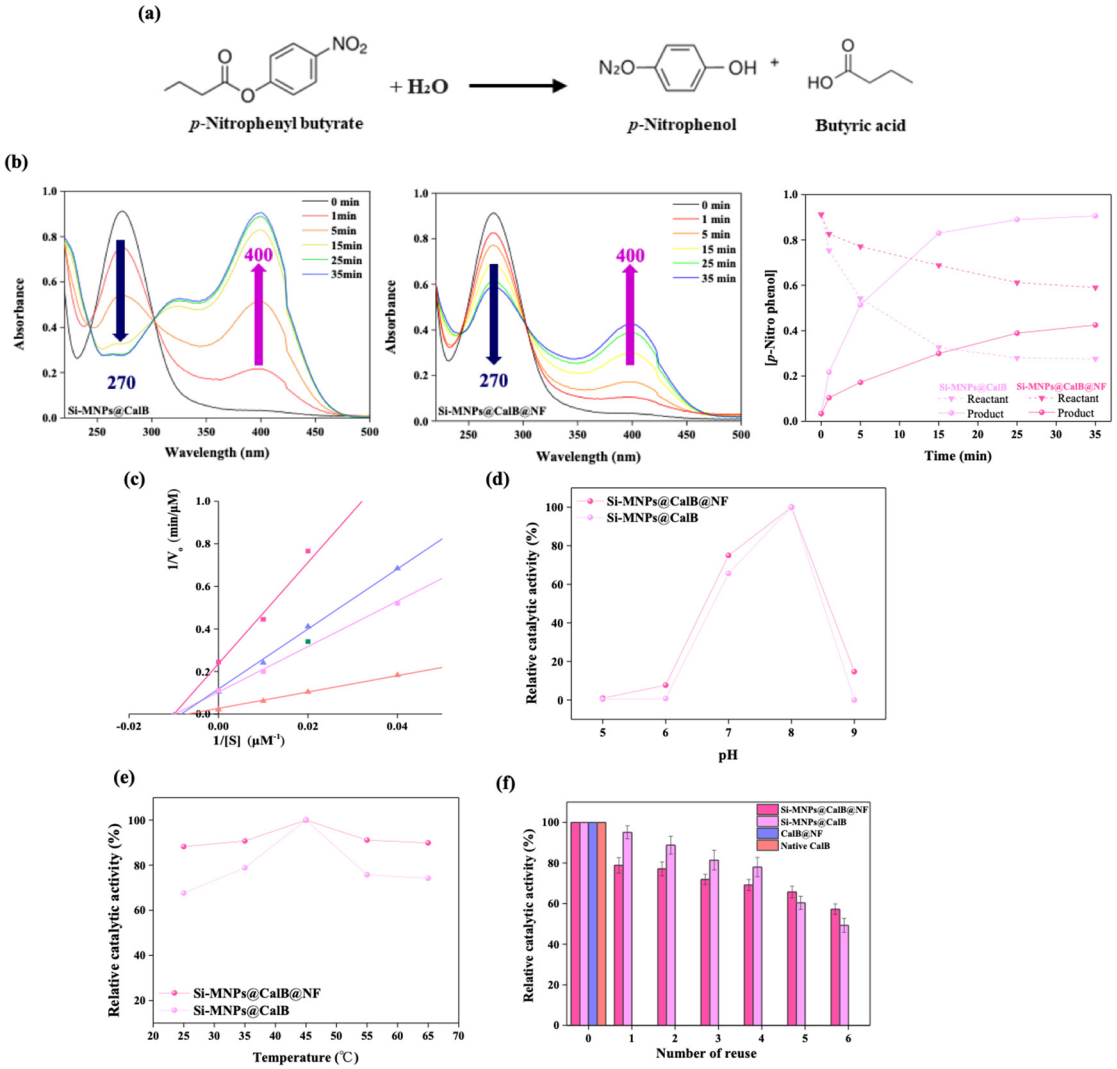

Figure 2. (a) Schemes of enzymatic hydrolysis against *p*-NPB to *p*-NP, (b) absorbance spectrum of *p*-NPB hydrolysis with Si-MNPs@CalB and Si-MNPs@CalB@NF as a function of time, (c) Lineweaver-Burk plot with native CalB, CalB@NF, Si-MNPs@CalB, and Si-MNPs@CalB@NF, respectively, (d) catalytic activity at different pH, (e) at different temperature, and (f) reusability of native CalB, CalB@NF, Si-MNPs@CalB, and Si-MNPsCalB@NF.

Table 1. Michaelis-Menten parameters with native CalB, CalB@NF, Si-MNPs@CalB, and Si-MNPs@CalB@NF.

	K_m (μM)	Vmax (μM·min^{-1})	K_{cat} (min^{-1})	K_{cat}/ K_m (μM^{-1}·min^{-1})
Native CalB	187	46	1391	7.4
CalB@NF	94	9	1909	20.3
Si-MNPs@CalB	139	9.5	1151	8.3
Si-MNPs@CalB@NF	96	4	975	10.2

2.3. Enzymatic Acylation

Figure 3 shows the synthesis and conversion efficiency of benzyl benzoate through enzyme synthesis. Figure 3a shows the reaction scheme for the acylation of benzyl benzoate from benzoic anhydride. The acylation reaction resulted in the synthesis of benzyl benzoate from benzoic anhydride using 0.5 g of enzyme from four samples (native CalB, CalB@NF, Si-MNPs@CalB, and Si-MNPs@CalB@NF). Benzoic acid is also produced from benzyl alcohol, which is used in the synthesis of benzyl benzoate. Figure 3b shows the results of the UV-Vis. analysis before and after column

 doi:10.20944/preprints202408.0671.v1

separation of the products of benzyl benzoate. As a result of the UV-Vis measurement after the reaction, benzoic acid was also detected in addition to benzyl benzoate, and column chromatography was performed. After column chromatography and UV-Vis measurement, the absorbance of benzyl benzoate shows peaks at λ_{ex}=200 nm and λ_{ex}=229 nm. From the UV-Vis analysis, the four samples showed the same peak at λ_{ex}=229 nm as benzyl benzoate, confirming its synthesis. Figure 3c shows the thin layer chromatography (TLC) measured to confirm the synthesis of benzyl benzoate using four samples. TLC was performed using standard reagents in the order of benzoic anhydride, benzyl alcohol, and benzyl benzoate, and the product was also separated and measured by column chromatography. The R_f values of benzyl alcohol and benzoic anhydride are 0.3 and 0.64, respectively, and the R_f value of benzyl benzoate is 0.9, and the products synthesized using four samples were also confirmed to have an R_f value of 0.9. Figure 3d shows the conversion efficiency of benzoic anhydride to benzyl benzoate. The conversion efficiency was calculated using the following equation:

$$\text{Conversion (\%)} = \frac{BA_i - BA_f}{BA_i} \times 100 \quad (1)$$

In the equation, BA_i and BA_f are the initial and final concentrations of benzoic anhydride, the reactant, before and after enzymatic synthesis, respectively. The conversion efficiencies were 99.1%, 99.1%, 99.4%, and 99.5% for native CalB, CalB@NF, Si-MNPs@CalB, and Si-MNPs@CalB@NF, respectively, with all values greater than 99%. This indicates that benzoic anhydride is suitable for the synthesis of benzyl benzoate.

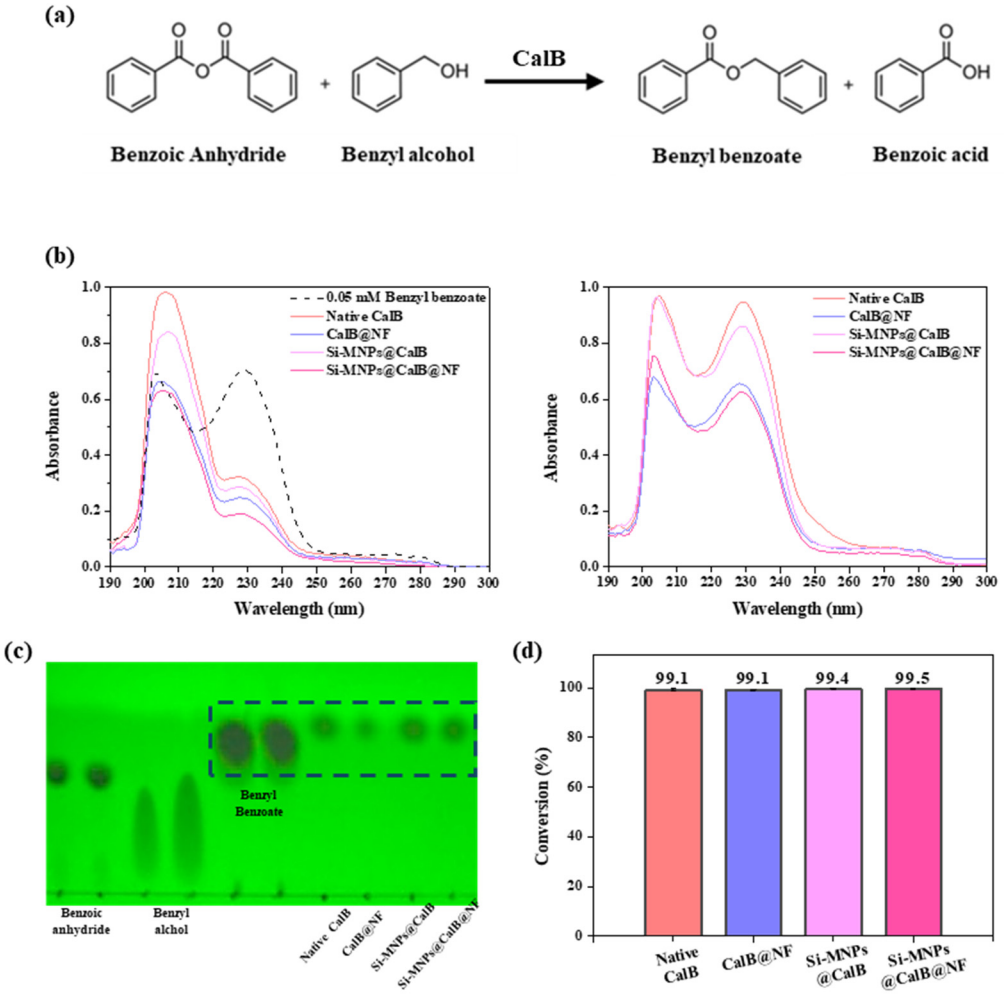

Figure 3. (a) Schemes of enzymatic acylation of benzyl benzoate with benzoic anhydride, (b) formed benzyl benzoate during enzymatic synthesis before and after column chromatography, (c) Thin layer

 doi:10.20944/preprints202408.0671.v1

chromatography (TLC), and (d) conversion efficiency of benzyl benzoate with native CalB, CalB@NF, Si-MNPs@CalB, and Si-MNPs@CalB@NF.

2.4. Enzymatic Lipolysis

Figure 4 shows the lipolysis and the concentration of decomposed fatty acids for the four samples (native CalB, CalB@NF, Si-MNPs@CalB, and Si-MNPs@CalB@NF). Figure 4a shows the process of lipolysis for the four samples. A triglyceride (TAG) is a molecular form in which three fatty acids are esterified to a glycerol molecule. These TAGs can be decomposed by lipases into fatty acids and glycerol. The TAG used in this study is olive oil. The decomposition to oleic acid was confirmed using olive oils, which contain up to 83% oleic acid content. The reason for using vegetable oils high in oleic acid is that oleic acid is highly stable, which prevents it from interfering with the enzymes during the lipolysis reactions. The amount of enzyme used for decomposition was a quantitative result according to the CalB content in Figure 1e, and samples of 6.7 g CalB@NF, 4.3 g Si-MNPs@CalB, and 8.6 g Si-MNPs@CalB@NF were used based on 1 g native CalB. Figure 4b shows TLC to confirm the product after the lipolysis reaction. Comparing the TLC of the product with the reactant, olive oil, and the four samples confirms that the TLC of the product has a new spot that did not appear for the reactant (olive oil). Since the experiment was conducted by identifying the amount of enzyme present, the size of the spot of the product was the same for the four samples.

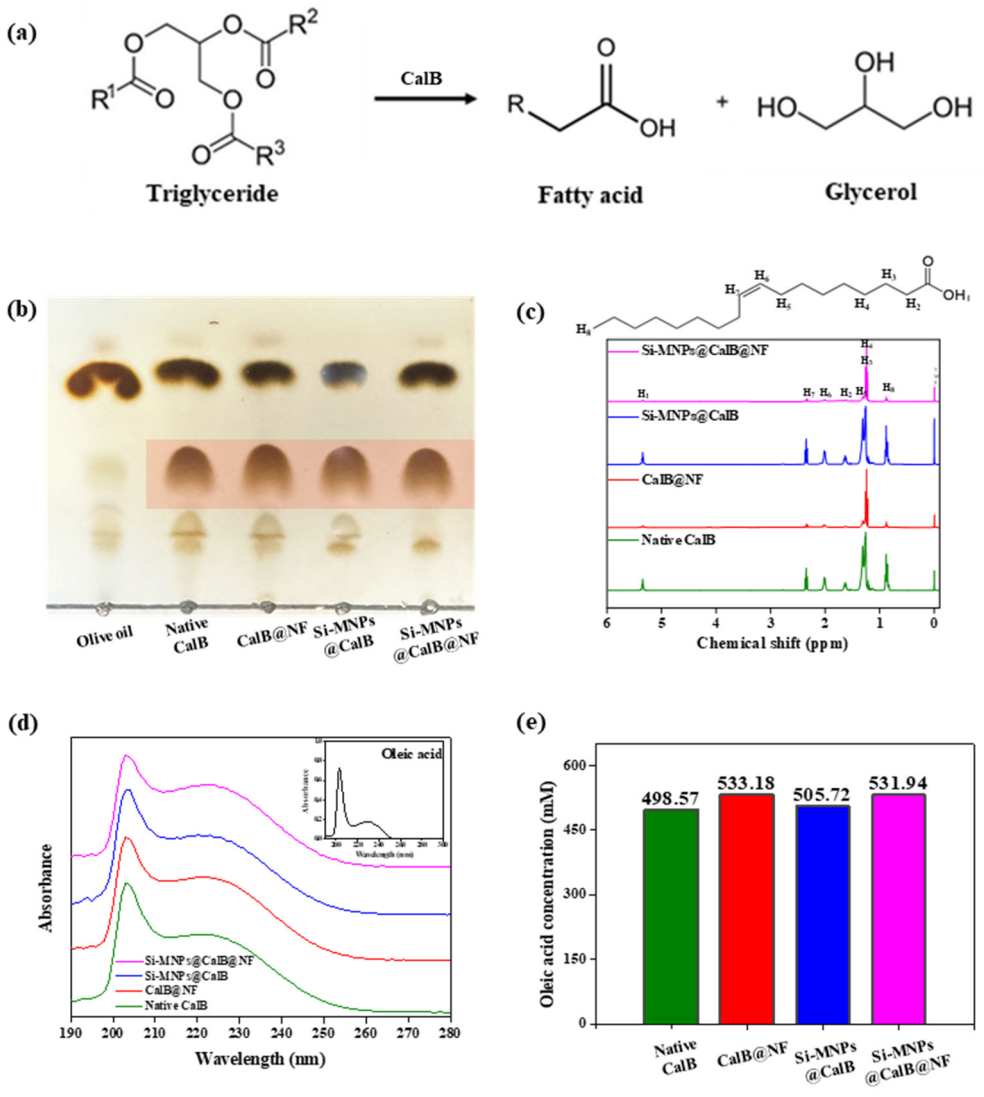

Figure 4. (a) Schemes of enzymatic lipolysis with olive oil, (b) thin layer chromatography (TLC), (c) ^{1}H-NMR after column chromatography, (d) UV-Vis spectra after column chromatography, and (e)

 doi:10.20944/preprints202408.0671.v1

oleic acid concentration after lipolysis with native CalB, CalB@NF, Si-MNPs@CalB, and Si-MNPs@CalB@NF.

To confirm the components of the new spot, it was separated by column chromatography and structural analysis was performed via a ^{1}H-NMR analysis. Figure 4c presents the results of the ^{1}H-NMR analysis showing the ^{1}H-NMR peaks of the oleic acid standard and the new spots generated by the lipolysis catalyzed reaction of native CalB, CalB@NF, Si-MNPs@CalB and Si-MNPs@CalB. ^{1}H NMR analysis at 400 MHz shows the ^{1}H NMR peaks of the oleic acid standard at 0.9 ppm (s, -CH_3, H_8), 1.27 ppm (s, -CH_2, H_4), 1.31 ppm (s, -CH_2, H_3), 1.35 ppm (s, -CH_2, H_6), 1.63 ppm (s, -CH_2, H_2), 2.01 ppm (s, =CH, H_6), 2.3 ppm (s, =CH, H_7), and 5.3 ppm (s, -OH, H_1). By analyzing the ^{1}H-NMR spectra of the oleic acid standards and the peaks corresponding to the products of native CalB, CalB@NF, Si-MNPs@CalB and Si-MNPs@CalB, we observed strong agreement between them. However, we cannot overlook that the solvent used in the samples was less purified and may have affected the results. The UV-Vis analyses of each ^{1}H-NMR determined sample are shown in Figure 4d. We also determined the oleic acid concentration in each sample using UV-Vis. The oleic acid UV-Vis results of the 0.025 mM standard reagent are shown at the top right. The UV-Vis spectrum of oleic acid appears at λ_{ex} =230 nm and a calibration with R^2=0.999 was drawn. Therefore, the lipolysis product of the four samples was diluted 10,000 times for the UV-Vis analysis. The products of all four samples showed the same peak at λ_{ex}=230 nm as oleic acid reagent in the purified spot. Figure 4e shows the concentration of the generated oleic acid based on the calibration curve obtained using the oleic acid reagent. The concentrations of produced oleic acid were 498.57 mM, 533.18 mM, 505.72 mM, and 531.94 mM for native CalB, CalB@NF, Si-MNPs@CalB, and Si-MNPs@CalB@NF, respectively, confirming that all four samples produced approximately 500 mM of oleic acid. Native CalB, a representative lipolytic enzyme, demonstrated efficient fat decomposition. Similarly, CalB@NF also exhibited effective lipid degradation. Both enzymes have demonstrated the ability to perform lipolysis even when immobilized, and considering their reusability, Si-MNPs@CalB and Si-MNPs@CalB@NF are anticipated to have useful applications in industry.

3. Materials and Methods

3.1. Materials

Ferric chloride hexahydrate ($FeCl_3 \cdot 6H_2O$), ferrous chloride tetrahydrate ($FeCl_2 \cdot 4H_2O$), tetraethyl orthosilicate (99%, TEOS), polyoxyethylene nonylphenylether (Igepal® CO-520), oleic acid, ammonium hydroxide, chloroform, acetic acid, p-nitrophenyl butyrate (≥98%, *p*-NPB), benzoic anhydride, benzoic acid, benzyl alcohol, trizma base, phosphate buffer saline (PBS), bovine serum albumin (BSA), Coomassie brilliant blue reagent, and petroleum ether were purchased from Sigma-Aldrich (Korea). Cyclohexane, toluene, ethanol, methanol, hexane, ethyl acetate, ethyl ether and hydrochloric acid were purchased from Daejeong (Korea). *Candida antarctica* lipase B (CalB) and nano-fructosome Candida antarctica lipase B (CalB@NF) were provided by the Korea Research Institute of Bioscience & Biotechnology (KRIBB, Korea). 3-chloropropyltriethoxysilane was purchased from Gelest (USA). Other chemicals were of analytical grade.

3.2. The Preparation of MNPs and Si-MNPs

The MNPs were prepared by the co-precipitation method [42]. A mixture of iron (II) chloride tetrahydrate aqueous solution (2 M) and iron (III) chloride hexahydrate aqueous solution (1 M) was stirred, and NH_4OH solution (0.7 M) was added to the stirred solution. The obtained MNPs were collected using a magnet, washed with ethanol and dried at room temperature. Si-MNPs were prepared by the Stöber process [43]. MNPs (90 mg) and oleic acid (2 mL) in cyclohexane (120 mL) were dispersed by ultra-sonication. A stirred solution of Igepal® CO-520 (24 g) in cyclohexane (300 mL) was added and stirred, and TEOS was slowly added dropwise to the stirred solution. Finally, 28-30% NH_4OH (163 mL) was added and stirred for 24 hours at room temperature. After the reaction was completed, methanol (325 mL) was added to the solution to separate the supernatant and

 doi:10.20944/preprints202408.0671.v1

precipitate, and the Si-MNPs were collected using a magnet. The collected Si-MNPs were washed, and then vacuum dried for 24 hours.

3.3. Immobilization of Native CalB & CalB@NF Lipase on Si-MNPs

Si-MNPs (500 mg) were added to toluene (100 mL), stirred, and distilled water (0.125 g) was added dropwise. The temperature was raised to 60 °C, 3-chloropropyltriethoxysilane (0.65 g) was added dropwise, and the temperature was raised to 110 °C and the solution was refluxed for 24 hours. After the reaction was completed, the Si-MNPs@Cl obtained with a magnet was washed with distilled water and ethanol and dried under vacuum. The prepared Si-MNPs@Cl (50 mg) was dispersed in cyclohexane (20 mL), and then native CalB and CalB@NF were added to disperse it. The dispersed mixture was reacted on a roller at room temperature for 24 h. After the reaction was completed, the product Si-MNPs@enzyme was washed with cyclohexane and vacuum dried for 24 hours.

3.4. Bradford Assay

A calibration curve was generated by mixing a stepwise diluted solution of bovine serum albumin (BSA) in PBS solution (pH 7) (0.1 mL) with Coomassie Blue G-250 (0.9 mL) and measuring the absorbance under UV-Vis (λ_{ex}=595 nm). Native CalB, CalB@NF, Si-MNPs@CalB and Si-MNPs@CalB@NF (1 mg) were placed in an electron tube, followed by the addition of PBS buffer (1 mL) and centrifuging. The separated supernatant (0.1 mL) was mixed in Coomassie Blue (0.9 mL) and protein was quantified by measuring the absorbance under UV-Vis (λ_{ex}=595 nm) [44,45].

3.5. Enzymatic Hydrolysis, Acylation, and Lipolysis

The catalytic hydrolysis of *p*-NPB against native CalB, CalB@NF, Si-MNPs@CalB, and Si-MNPs@CalB@NF was conducted as follows. A *p*-NPB solution (1 mM) was prepared using Tris-HCl buffer (pH 7) and each sample (0.1 mg) was added to the prepared p-NPB solution (1 mL), mixed and reacted, centrifuged, and absorbance (λ_{ex}=270 and 400 nm) was measured under UV-Vis. The catalytic parameters (Michaelis-Menten constants) of native CalB, CalB@NF, Si-MNPs@CalB, and Si-MNPs@CalB@NF were calculated by measuring the initial linear velocity using a Lineweaver-Burk power law plot.

$$\frac{1}{V_o} = \frac{K_m}{V_{max}} \times \frac{1}{[S]} + \frac{1}{V_{max}} \quad (2)$$

where K_m and V_{max} are the Michaelis-Menten constant (μM) and maximum rate (μM·min^{-1}), respectively. [S] and V_0 are the substrate concentration (μM) and reaction rate (μM·min^{-1}), respectively. Independent measurements were performed for the substrate concentrations. The catalytic acylation of benzoic anhydride to native CalB, CalB@NF, Si-MNPs@CalB and Si-MNPs@CalB@NF was conducted as follows. Benzyl anhydride was dissolved in benzyl alcohol at a concentration of 9:1, and native CalB, CalB@NF, Si-MNPs@CalB, and Si-MNPs@CalB@NF (0.5 g) were added to the dissolution solution, respectively, and stirred at 50 °C for 20 hours. After the reaction, the supernatants were separated by centrifugation and analyzed by thin layer chromatography (TLC). The solvent was evaporated using a rotary evaporator and the concentrated solution was subjected to column chromatography to isolate the desired compound. The formation of benzyl benzoate was determined by measuring the absorbance via UV-Vis (λ_{ex}=229 nm). The catalytic lipolysis of olive oil to native CalB, CalB@NF, Si-MNPs@CalB and Si-MNPs@CalB@NF was conducted as follows. Tris-HCl buffer (pH 8, 50 mM, 0.5 mL) was added to olive oil (10 mL) and stirred at 45°C for 1 hour at 1000 rpm. Tris-HCl buffer (9.5 mL) and enzymes (native CalB, CalB@NF, Si-MNPs@CalB, Si-MNPs@CalB@NF) were added in separate containers and stirred for one hour. Enzyme buffer was added to the hydration reaction solution and stirred at 45°C at 1000 rpm for 24 hours. After stirring, the supernatant and precipitate were separated by centrifugation for analysis.

 doi:10.20944/preprints202408.0671.v1

3.6. pH and Thermal Stability, and Reusability

The pH activity was measured at pH = 5, 6, 7, 8, and 9, and *p*-NPB solution (0.1 M) was prepared after buffers were prepared for each pH. Si-MNPs@CalB and Si-MNPs@CalB@NF were added to the corresponding buffer (1 mL) at a concentration of 1 mg/mL, respectively, and after 1 min, the samples were centrifuged (15,000 rpm, 10 s). The supernatant (0.1 mL) was mixed with *p*-NPB buffer (0.1 mM, 0.9 mL) and after 5 min, the absorbance was measured using UV-Vis. (λ_{ex}=400 nm). Thermal stability was evaluated at 25℃, 35℃, 45℃, 55℃ and 65℃. *p*-NPB solution (0.1 mM) was prepared using Tris-HCl buffer (pH 7). The *p*-NPB solution (1 mL) was heated to the specified evaluation temperature, and Si-MNPs@CalB and Si-MNPs@CalB@NF were added to Tris-HCl buffer (1 mL) at a concentration of 1 mg/mL. After 1 min the samples were centrifuged (15,000 rpm, 10 s) and the supernatant (0.1 mL) was mixed with *p*-NPB buffer (0.1 mM, 0.9 mL) and after 5 min the absorbance was measured using UV-Vis (λ_{ex}=400 nm). Reusability was determined by preparing *p*-NPB solution (0.1 mM) using Tris-HCl buffer (pH 7) and adding *p*-NPB solution (0.1 mM, 1 mL) to Si-MNPs@CalB and Si-MNPs@CalB@NF (1 mg), respectively. The mixture was then incubated for 5 min and centrifuged. The absorbance was measured using UV-Vis (λ_{ex}=400 nm). The sample was then washed with Tris-HCl buffer (pH 7) and the process repeated.

3.7. Instrumental Analysis

The morphological details of MNPs and Si-MNPs were evaluated by JEM-2100Plus transmission electron microscope (TEM) (JEOL, Tokyo, Japan) at an accelerating voltage of 200 kV. The magnetization of MNPs and Si-MNPs was measured using VSM (Lake Shore, Model 7404, USA) at room temperature (maximum of 1 T and 300 K). Fourier transform infrared (FT-IR) spectroscopy was carried out for identification and characterization of MNPs, Si-MNPs, and Si-MNPs@Cl. FT-IR spectra were measured with a KBr compressed pellet in wavelength range of 750–4000 cm^{-1} using an SDT Q600 Frontier (Perkin Elmer, Houston, TX, USA). To evaluate the amount of enzyme immobilized on Si-MNPs@Cl, thermogravimetric analysis (TGA) was performed using a Q600 TA instrument (Waters, Milford, MA, USA) from room temperature to 700 °C at a heating rate of 10 °Cmin^{-1} in a nitrogen atmosphere. UV-Visible spectrophotometry was measured by Mega 900 (SCINCO, Seoul, Korea) in a range of 190–500 nm. ^{1}H-NMR spectra were measured on a Bruker Advance III 400 spectrometer (400 MHz) (Chungbuk, Korea) using $CDCl_3$ solutions and TMS as an internal standard. Chemical shifts are reported in parts per million (ppm, d) relative to the internal tetramethyl silane standard (TMS, d 0.00). Column chromatography was typically performed on silica gel (pore size 60 Å, particle size 32-63 nm), and reactions were monitored by thin-layer chromatography (TLC) analysis performed with Merck Kiese gel 60 F254 plates and visualized with UV light at 240 nm and by burning10% sulfuric acid.

4. Conclusion

The silica coating of silica-coated magnetic nanoparticles (Si-MNPs) was achieved through the sol-gel method using TEOS. The resulting Si-MNPs were analyzed via TEM, revealing a uniform spherical shape with a size of 60 nm. The coated magnetic nanoparticles were surface treated using -Cl silane. Enzyme immobilization was performed with native CalB and CalB@NF on Si-MNPs@Cl at 1:1 (w/w) each. Proteins were quantified using a Bradford assay, resulting in a ratio of 7:1 for native CalB: CalB@NF and a ratio of 2:1 for Si-MNPs@CalB: Si-MNPs@CalB@NF. Compared to native CalB, CalB@NF demonstrated stability over a wide range of pH and temperature conditions. It was confirmed that Si-MNPs@CalB and Si-MNPs@CalB@NF could be reused, whereas native CalB and CalB@NF could not. This has also been demonstrated in the enzymatic hydrolysis of *p*-NPB, the enzymatic synthesis of benzyl benzoate, and the enzymatic lipolysis of vegetable oil. Enzymatic hydrolysis showed that *p*-NPB was converted to *p*-NP on the basis of Lineweaver-Burk plots and Michaelis-Menten kinetics. Enzymatic acylation showed that almost all benzoic anhydride was converted to benzyl benzoate with conversion efficiencies over 99% for native CalB, CalB@NF, Si-MNPs@CalB, and Si-MNPs@CalB@NF. Finally, the results of olive oil lipolysis showed that all four

 doi:10.20944/preprints202408.0671.v1

samples were decomposed to about 500 mM oleic acid. Thus, CalB@NF is more stable against temperature changes than native CalB, and Si-MNPs@CalB and Si-MNPs@CalB@NF are reusable in contrast to native CalB and CalB@NF. These findings are expected to result in significant cost savings as is less susceptible to environmental changes and can be applied in continuous processes.

Author Contributions: Conceptualization, J.H.C.; methodology, J.H.C.; data curation, Y.J.K; writing—original draft preparation, Y.J.K.; writing—review and editing, J.H.C.; supervision, J.H.C.; project administration, J.H.C.; funding acquisition, J.H.C. All authors have read and agreed to the published version of the manuscript.

Funding: This work was supported by "Cooperative Research Program for Agriculture Science and Technology Development (Project No. PJ01493802)" Rural Development Administration, Republic of Korea.

Conflicts of Interest: The authors declare no conflict of interest.

References

1. Schoemaker, H. E.; Mink, D.; Wubbolts, M. G. Dispelling the myths-biocatalysis in industrial synthesis. *Science*, **2003,** 299, 1694-1697.
2. Soldatkin, O.; Kucherenko, I.; Pyeshkova, V.; Kukla, A.; Jaffrezic-Renault, N.; El'Skaya, A.; Dzyadevych, S.; Soldatkin, A. Novel conductometric biosensor based on three-enzyme system for selective determination of heavy metal ions. *Bioelectrochemystry.* **2012**, 83, 25-30.
3. Lee, H. R.; Kim, M. I.; Hong, S. E.; Choi, J.; Kim, Y. M.; Yoon, K. R.; Lee, S.; Ha, S. H. Effect of functional group on activity and stability of lipase immobilized on silica-coated magnetite nanoparticles with different functional group. *J. Anal. Sci. Technol.* **2016**, 29 (3), 105-113.
4. Stauch, B.; Fisher, S. J.; Cianci, M. Open and closed states of Candida antarctica lipase B: Protonation and the mechanism of interfacial activation1. *J. Lipid Res.* **2015**, 56 (12), 2348-2358.
5. Cho, C. H.; Patel, S.; Rajbhandari, P. Adipose tissue lipid metabolism: lipolysis. *Curr. Opin. Genet. Dev.* **2023**, 83, 102114.
6. Vaughan, M.; Berger, J. E.; Steinberg, D. Hormone-sensitive lipase and monoglyceride lipase activities in adipose tissue. *J. Biol. Chem.* **1964**, 239 (2), 401-409.
7. Wu, Q.; Soni, P.; Reetz, M. T. Laboratory evolution of enantiocomplementary Candida antarctica lipase B mutants with broad substrate scope. *J. Am. Chem. Soc.* **2013**, 135 (5), 1872-1881.
8. Basso, A.; Serban, S. Industrial applications of immobilized enzymes—A review. *Mol. Catal.* **2019**, 479, 110607.
9. Khan, N. R.; Rathod, V. K. Enzyme catalyzed synthesis of cosmetic esters and its intensification: A review. *Process Biochem.* **2015**, 50 (11), 1793-1806
10. Salihu, A.; Alam, M. Z. Solvent tolerant lipases: a review. *Process Biochem.* **2015**, 50 (1), 86-96.
11. Navvabi, A.; Razzaghi, M.; Fernandes, P.; Karami, L.; Homaei, A. Novel lipases discovery specifically from marine organisms for industrial production and practical applications. *Process Biochem.* **2018**, 70, 61-70.
12. Angajala, G.; Pavan, P.; Subashini, R. Lipases: An overview of its current challenges and prospectives in the revolution of biocatalysis. *Biocatal. Agric. Biotechnol.* **2016**, 7, 257-270.
13. Lima, R. N.; dos Anjos, C. S.; Orozco, E. V.; Porto, A. L. Versatility of Candida antarctica lipase in the amide bond formation applied in organic synthesis and biotechnological processes. *Mol. Catal.* **2019**, 466, 75-105.
14. Li, N. W.; Zong, M. H.; Wu, H. Highly efficient transformation of waste oil to biodiesel by immobilized lipase from Penicillium expansum. *Process Biochem.* **2009**, 44 (6), 685-688.
15. SÁ, A. G. A.; de Meneses, A. C.; de Araújo, P. H. H.; de Oliveira, D. A review on enzymatic synthesis of aromatic esters used as flavor ingredients for food, cosmetics and pharmaceuticals industries. *Trends Food Sci. Technol.* **2017**, 69, 95-105.
16. Guo, Y.; Cai, Z.; Xie, Y.; Ma, A.; Zhang, H.; Rao, P.; Wang, Q. Synthesis, physicochemical properties, and health aspects of structured lipids: A review. *Compr. Rev. Food Sci. Food Saf.* **2020**, 19 (2), 759-800.
17. Mulinari, J.; Oliveira, J. V.; Hotza, D. Lipase immobilization on ceramic supports: An overview on techniques and materials. *Biotechnol. Adv.* **2020**, 42, 107581.
18. Ghanem, A. Trends in lipase-catalyzed asymmetric access to enantiomerically pure/enriched compounds. *Tetrahedron* **2007**, 63 (8), 1721-1754.
19. Sun, J.; Jiang, Y.; Zhou, L.; Gao, J. Immobilization of Candida antarctica lipase B by adsorption in organic medium. *New Biotechnol.* **2010**, 27 (1), 53-58.
20. Adlercreutz, P. Immobilisation and application of lipases in organic media. *Chem. Soc. Rev.* **2013**, 42 (15), 6406-6436.
21. Kirk, O.; Christensen, M. W. Lipases from candida a ntarctica: unique biocatalysts from a unique origin. *Org. Process Res. Dev.* **2002**, 6 (4), 446-451.
22. Monteiro, R. R.; Neto, D. M. A.; Fechine, P. B.; Lopes, A. A.; Gonçalves, L. R.; Dos Santos, J. C.; de Souza, M. C.; Fernandez-Lafuente, R. Ethyl butyrate synthesis catalyzed by lipases A and B from Candida

 doi:10.20944/preprints202408.0671.v1

antarctica immobilized onto magnetic nanoparticles. Improvement of biocatalysts' performance under ultrasonic irradiation. *Int. J. Mol. Sci.* **2019**, 20 (22), 5807.
23. Mangiagalli, M.; Carvalho, H.; Natalello, A.; Ferrario, V.; Pennati, M. L.; Barbiroli, A.; Lotti, M.; Pleiss, J.; Brocca, S. Diverse effects of aqueous polar co-solvents on Candida antarctica lipase B. *Int. J. Biol. Macromol.* **2020**, 150, 930-940.
24. Hundschell, C.; Jakob, F.; Wagemans, A. Molecular weight dependent structure of the exopolysaccharide levan. *Int. J. Biol. Macromol.* **2020**, 161, 398-405.
25. Arvidson, S. A.; Rinehart, B. T.; Gadala-Maria, F. Concentration regimes of solutions of levan polysaccharide from Bacillus sp. *Carbohydr. Polym.* **2006**, 65 (2), 144-149.
26. Sonh, J. H.; Bae, J. H. Levan-Protein Nanocomposite and Uses Thereof. KR Patent **2021**, 10, 0012979.
27. Rotticci, D.; Rotticci-Mulder, J. C.; Denman, S.; Norin, T.; Hult, K. Improved enantioselectivity of a lipase by rational protein engineering. *ChemBioChem.* **2001**, 2 (10), 766-770.
28. Hartmann, M.; Kostrov, X. Immobilization of enzymes on porous silicas–benefits and challenges. *Chem. Soc. Rev.* **2013,** 42 (15), 6277-6289.
29. Sun, J.; Zhang, H.; Tian, R.; Ma, D.; Bao, X.; Su, D. S.; Zou, H. Ultrafast enzyme immobilization over large-pore nanoscale mesoporous silica particles. *Chem. Commun.* **2006**, (12), 1322-1324..
30. Montiel, M.; Serrano, M.; Máximo, M.; Gómez, M.; Ortega-Requena, S.; Bastida, J. Synthesis of cetyl ricinoleate catalyzed by immobilized Lipozyme® CalB lipase in a solvent-free system. *Catal. Today* **2015**, 255, 49-53.
31. Neupane, S.; Patnode, K.; Li, H.; Baryeh, K.; Liu, G.; Hu, J.; Chen, B.; Pan, Y.; Yang, Z. Enhancing enzyme immobilization on carbon nanotubes via metal–organic frameworks for large-substrate biocatalysis. *ACS Appl. Mater. Interfaces* **2019**, 11 (12), 12133-12141.
32. Bartczak, D.; Kanaras, A. G. Preparation of peptide-functionalized gold nanoparticles using one pot EDC/sulfo-NHS coupling. *Langmuir* **2011**, 27 (16), 10119-10123.
33. Tang, W.; Ma, T.; Zhou, L.; Wang, G.; Wang, X.; Ying, H.; Chen, C.; Wang, P. Polyamine-induced tannic acid co-deposition on magnetic nanoparticles for enzyme immobilization and efficient biodiesel production catalysed by an immobilized enzyme under an alternating magnetic field. *Catal. Sci. Technol.* **2019**, 9 (21), 6015-6026.
34. Lee, S. Y.; Ahn, C. Y.; Lee, J.; Chang, J. H. Amino acid side chain-like surface modification on magnetic nanoparticles for highly efficient separation of mixed proteins. *Talanta* **2012**, 93, 160-165.
35. Hazarika, K. P.; Borah, J. Study of biopolymer encapsulated Eu doped Fe3O4 nanoparticles for magnetic hyperthermia application. *Sci. Rep.* **2024**, 14 (1), 9768.
36. Gupta, A. K.; Gupta, M. Synthesis and surface engineering of iron oxide nanoparticles for biomedical applications. *Biomater.* **2005**, 26 (18), 3995-4021.
37. Křížová, J.; Španová, A.; Rittich, B.; Horák, D. Magnetic hydrophilic methacrylate-based polymer microspheres for genomic DNA isolation. *J. Chromatogr. A* **2005**, 1064 (2), 247-253.
38. Lee, S. Y.; Lee, J. H.; Chang, J. H.; Lee, J. H. Inorganic nanomaterial-based biocatalysts. *BMB Rep*. **2011**, 44 (2), 77-86.
39. Tran, D. T.; Chen, C. L.; Chang, J. S. Immobilization of Burkholderia sp. lipase on a ferric silica nanocomposite for biodiesel production. *J. Biotechnol.* **2012**, 158 (3), 112-119.
40. Mehrasbi, M. R.; Mohammadi, J.; Peyda, M.; Mohammadi, M. Covalent immobilization of Candida antarctica lipase on core-shell magnetic nanoparticles for production of biodiesel from waste cooking oil. *Renewable energy* **2017**, 101, 593-602.
41. Kim, S. H.; Sung, D. K.; Chang, J. H. Highly efficient antibody purification with controlled orientation of protein A on magnetic nanoparticles. *MedChemComm* **2017,** 1, 108–112.
42. Lee, S. Y.; Lee, S. Y.; Lee, J. H.; Lee, H. S.; Chang, J. H. Biomimetic magnetic nanoparticles for rapid hydrolysis of ester compounds. *Materials Letters* **2013,** 110, 229-232.
43. Mylkie, K.; Nowak, P.; Rybczynski, P.; Ziegler-Borowska, M. Polymer-Coated Magnetite Nanoparticles for Protein Immobilization. *Materials* **2021**, 14 (2), 248.
44. Kruger, N. J. The Bradford method for protein quantitation. The protein protocols handbook **2009**, 17-24.
45. Bradford, M. M. A rapid and sensitive method for the quantitation of microgram quantities of protein utilizing the principle of protein-dye binding. Anal. Biochem. **1976**, 72 (1-2), 248-254.